Surfaces and Interfaces 9 (2017) 160–166

Contents lists available at ScienceDirect

Surfaces and Interfaces

journal homepage: www.elsevier.com/locate/surfin

Effect of different copper salts on the electrochemical determination of Cu (II) by the application of the graphene oxide-modified glassy carbon electrode

Hilal İncebay[a], Zafer Yazıcıgil[b,*]

[a] Nevsehir Hacı Bektas Veli University, Faculty of Arts and Sciences, Department of Chemistry, Nevsehir, Turkey
[b] Selcuk University, Faculty of Science, Department of Chemistry, Konya, Turkey

ARTICLE INFO

Keywords:
Cu(II) determination
Graphene oxide
Chemical reduction
Metal sensor

ABSTRACT

In this study, graphene oxide and reduced graphene oxide nanoparticles were synthesized by Hummers method and characterized Fourier transform infrared spectroscopy, X-ray diffraction spectroscopy, scanning electron microscopy and thermogravimetric analysis. Then, glassy carbon electrode surfaces were modified with synthesized and characterized graphene oxide (GO) and reduced graphene oxide (red-GO) using physical immobilization. Bare and modified surfaces were characterized by cyclic voltammetry, electrochemical impedance spectroscopy and scanning electron microscopy. Application of graphene oxide (GO/GC) and reduced graphene oxide-modified glassy carbon (red-GO/GC) surfaces for the electrochemical determination of copper(II) using different copper salts such as $CuSO_4{\cdot}5H_2O$, $Cu(NO_3)_2{\cdot}3H_2O$ and $CuCl_2$ were performed by differential pulse voltammetry. The GO/GC surface was found to be suitable for selective determination of Cu(II) in the solutions containing the mixture of heavy metal ions (Zn(II), Pb(II), Cd(II), Fe(III) and Mn(II)) and showed high stability and reproducibility. The GO/GC surface was treated with $CuSO_4{\cdot}5H_2O$, $Cu(NO_3)_2{\cdot}3H_2O$ and $CuCl_2$ salts solution in optimum conditions and afterward SEM images were measured 10 μm in size and radius of these ions in Cu (II)/GO/GC surfaces. Thus the determination of copper ions on the GO/GC surface was made for the first time by comparing the effect of the types of copper salts. When it was evaluated in terms of inorganic theory, the results were found to be in harmony.

1. Introduction

Heavy metal ions have great importance in living organisms. However, the amounts may cause serious problems to the environment and human health [1]. For example, copper is an agent that is found very abundantly in nature and is spread as a result of natural events. It is one of the transition metals essential to human health and vital to all living organisms [2,3]. However, exposure to excess copper ions can cause some diseases including Wilson's disease, Menkes syndrome, Alzheimer's disease, neurodegenerative diseases, cancer, and amyotrophic lateral sclerosis [4–8]. Furthermore, copper pollution is much more serious in industrialized societies because of increasing industrial emissions and the toxicity of metal ions in drinking water [8]. For this reason, several effective methods are available for copper ion determination. It also has received considerable attention due to its use in material science and chemical industries [9,10]. Typical analysis methods for heavy metals such as spectroscopic [11,12], colorimetric [13–15], and fluorescent [16,17] techniques are very time consuming and noneconomic. Therefore, electrochemical techniques have an important place because of their high sensitivity, low cost, straightforward operation and ease of miniaturization [17–20]. In particular, with the development of nanomaterial science, carbon nanostructure based electrochemical systems are giving new inputs to novel heavy metal sensors of interest for applications in environmental, health and other fields [21–25].

Graphene oxide (GO), which is one of the carbon nanostructure family, is a known monolayer of carbon atoms that form dense honeycomb structures containing hydroxyl and epoxide functional groups on the two accessible sides and carboxylic groups at the edges [26,27]. Moreover, these extremely thin carbon nanostructures possess unique properties, including a large surface area for molecular adsorption, high conductivity, low cytotoxicity and easy functionalization [28]. Therefore, GO and its composites have a wide range of potential applications on solar cells [29,30], energy storage [31,32], telecommunications [33], robot construction [34,35], bioengineering and biomaterials areas [36,37], and nanoelectronics [38,39]. In recent years GO, which has

* Corresponding author.
E-mail addresses: hilalincebay@gmail.com (H. İncebay), zyazicigil@gmail.com (Z. Yazıcıgil).

http://dx.doi.org/10.1016/j.surfin.2017.09.004
Received 5 July 2017; Received in revised form 8 September 2017; Accepted 11 September 2017
Available online 12 September 2017

been the subject of many fields of study, also has an important role in the adsorption of metal ions [40]. GO has great potential for the adsorption of metal ions through its functional groups containing oxygen [41]. The adsorption of metal ions on the GO surface is carried out by physical or chemical adsorption depending on the kind of functional groups. Thus it can form a metal complex with electron pair sharing of metal ions with functional groups containing oxygen on the GO surface. Furthermore, the large surface area of GO leads to high adsorption capacity [42]. So GO can be used as an economical and practical adsorbent for metal adsorption.

In this work, graphene oxide and reduced graphene oxide were synthesized using Hummers method [43] and applied for the modification of glassy carbon electrode surfaces. Modified surfaces were used for the electrochemical determination of copper(II) from $CuSO_4{\cdot}5H_2O$, $Cu(NO_3)_2{\cdot}3H_2O$ and $CuCI_2$ salts for the first time in optimal conditions.

2. Experimental

All chemicals used in this study were of analytical grade and were purchased from the Merck, Riedel and Sigma–Aldrich companies.

Graphene oxide (GO) was synthesized from graphite powder by Hummers method [43]. To perform the synthesis, 69.0 mL H_2SO_4 and 3.0 g graphite powder were mixed at room temperature. At 0 °C, 9.0 g $KMnO_4$ was slowly added in portions to keep the reaction temperature below 20 °C. The reaction temperature was increased to 30-35 °C and stirred for 30 min then 138.0 mL of ultrapure water was slowly added in order to prevent a sudden temperature increase. External heating was introduced to maintain the reaction temperature at 95–98 °C for 15 min then the reaction heat was decreased to room temperature using a water bath for 10 min. Then 420.0 mL of ultrapure water and 3.0 mL of 30% H_2O_2 were added to the mixture and centrifuged at 5000 rpm at room temperature then washed repeatedly with ultrapure water to neutralize. Finally, the bright brown precipitate was dried for 24 h at 50 °C.

Reduced graphene oxide (red-GO) was synthesized from graphene oxide sheets [27]. For the preparation of graphene oxide plates, the 0.1 g of obtained GO plates was dispersed in 100 mL ultrapure water with ultrasonic vibration for 2 h. Then hydrazine (hydrazine:GO = 1:8 in weight) was added to obtain a black suspension of reduced graphene oxide sheets by stirring at 95 °C. Finally, the resultant black product was filtered and dried at 50 °C for 24 h.

The commercial graphite powder, synthesized GO and red-GO were characterized by Fourier transform infrared (FTIR-ATR) spectra (Bruker Vertex 70 spectrometer in the range 4000–400 cm^{-1} wavelength), X-ray diffraction (XRD) (Bruker D8 Advance X-ray diffractometer with CuKα radiation (λ = 1.54 Å) at a scanning rate of 0.05°/min in the 2θ range of 10–100°). Thermogravimetric analysis (TGA) of carbon nanostructures was also performed in an oxygen atmosphere at a heating rate of 10 °C/min from 30 °C to 500 °C using a Shimadzu TGDTA 60 thermal analyzer. The surface layers of these nanostructures were characterized by scanning electron microscopy (SEM-ZEISS LS-10 scanning electron microscope) without coating the nanostructures.

Prior to surface modification, the GC electrodes were cleaned according to previously published protocols [44–46]. Synthesized 1.0 mg GO and red-GO sheets were dispersed by sonication in 1.0 mL ultrapure water to form homogeneous suspensions (1.0 mg/mL). GO/GC and red-GO/GC electrodes were twice prepared separately dropwise with 5.0 μL GO and red-GO suspensions on bare GC electrode surfaces (0.071 cm^2) and evaporated for 1 h at room temperature.

Electrochemical measurements were performed in a three-electrode cell. GO/GC and rGO/GC were used as working electrodes, an Ag/AgCl in saturated KCl (Ag/AgCl/($KCl_{sat.}$)) as the reference electrode, and Pt wire as the counter electrode. Cyclic voltammetry (CV), electrochemical impedance spectroscopy (EIS), scanning electron microscopy (SEM), and differential pulse voltammetry (DPV) were conducted using a Gamry Reference 750 Potentiostat/Galvanostat from Gamry Instruments (PA, USA).

The bare GC, GO/GC and rGO/GC electrodes were characterized by CV, EIS and SEM methods. The characterization with CV was performed in a 1.0 mM ferricyanide solution prepared in BR buffer, pH 2.0, versus Ag/AgCl/KCl_{sat}. The cyclic voltammograms were recorded on bare GC, GO/GC and red-GO/GC electrodes in the potential range between +0.6/0.0 V at the scan rate of 100 mV/s. The characterization with EIS was performed in 100 mM KCl containing 1.0 mM of ferricyanide/ferrocyanide mixture. The Nyquist plots at bare GC, GO/GC and red-GO/GC electrodes were recorded at frequency ranges from 0.1 Hz to 75 kHz versus Ag/AgCl/KCl_{sat}.

In order to investigate electrochemical determination of copper(II) ions, GO/GC and rGO/GC surfaces were immersed in aqueous Cu(II) ions containing solutions prepared in different pH value of Britton–Robinson (BR) buffer solutions. The BR buffer was prepared by mixing of H_3BO_3, H_3PO_4, CH_3COOH and KCl stock solutions/chemicals then the pH was adjusted by addition of diluted NaOH or HCl solutions. Then, immersed electrodes were carefully washed with pure water and stable potential for the reduction of Cu(II) ions to metallic copper and anodic stripping was applied by differential pulse voltammetry (DPV), which was performed in the range of −0.3 V to +0.3 V versus Ag/AgCl/KCl_{sat} with a pulse amplitude of 50 mV, pulse time of 0.1 s, pulse period (interval) of 1 s and a voltage step of 2 mV in BR buffer solution, pH 5.0. Determination of Cu(II) ions was carried out separately by DPV technique using $CuSO_4{\cdot}5H_2O$, $Cu(NO_3)_2{\cdot}3H_2O$ and $CuCI_2$ salts solution. Then, the reproducibility test was performed using three different GC electrodes, which were prepared in the exact same conditions. Repeatability and stability tests were also performed using the same electrode for copper detection multiple times.

In order to investigate determination of selective Cu(II) ions on GO/GC, not only the effect of increasing concentrations (from 1 mM to 4 mM) of each of the different interference metals (Zn(II), Pb(II), Cd(II), Fe(III), Mn(II)) was examined respectively in BR buffer solution containing 1 mM Cu(II) ions, but also the individual effects of increased metal concentrations were investigated in the presence of the 1 mM interfering (Zn(II), Pb(II), Cd(II), Fe(III) and Mn(II)) metal ions together with 1 mM Cu(II) ions in BR buffer solution. For all experiments, the DPV technique was applied.

3. Results and discussion

3.1. Characterization of the synthesized GO and red-GO sheets

The prepared graphene oxide and reduced graphene oxide nanosheets were examined by Fourier transform infrared (FTIR) spectroscopy. The FTIR spectrum of GO nano sheets illustrated the presence of C−O (V_{C-O} at 1050 cm^{-1}), C=C ($V_{C=C}$ 1590–1620 cm^{-1}), and C=O ($V_{C=O}$ 1720–1740 cm^{-1}) (see Fig. 1a), [47–50]. An absorption band was observed at 3420 cm^{-1} for vibration of the OH group of water molecules [51]. Compared to GO, it was observed that a dramatic decrease in intensity of characteristic peaks of all the oxygen functional groups of red-GO nanosheets occurred because of the reduction with the hydrazine of GO. This showed that GO was almost completely reduced to graphene [52]. The reduction intensity of the peaks at 1730 cm^{-1}, 1620 cm^{-1} and 1050 cm^{-1} indicated that the epoxide and the hydroxyl groups attached to the basal graphene layer were removed.

XRD patterns of raw graphene, GO and red-GO are presented in Fig. 1b. GO exhibits a diffraction peak at 2θ = 12.47° corresponding to d spacing of 0.71 nm. This value is larger than the d-spacing (0.340 nm) of raw graphite powder (2θ = 26.49°) as a result of the intercalation of water molecules and the formation of oxygen-containing functional groups between the layers of graphite during oxidation [53]. In addition in raw graphite, a small peak at 54,7° was also observed for 0°0°4 plane. When the XRD peak of red-GO was evaluated it was seen that the

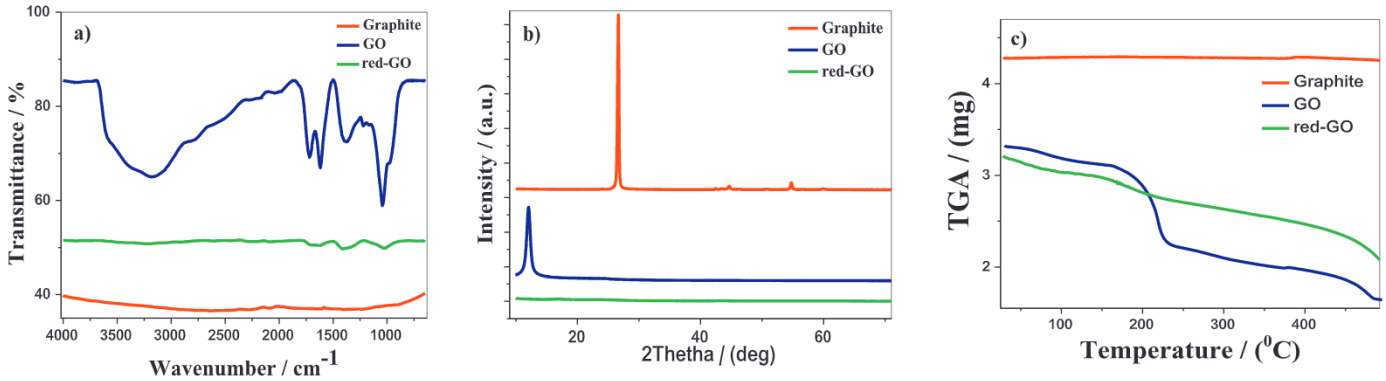

Fig. 1. Spectrum of (a) FTIR, (b) X-ray diffraction; (c) Thermogravimetric analysis of Graphite, GO and red-GO.

disappearance of the 0°0°2 reflection peak located at 12.47° and appearance of two weak and broad diffraction peaks at 17.5° and 14.0° suggested hybridization of sp^2 carbon was reestablished during the reduction, which is due to at 14.0° peak remain of some oxygen-containing functional groups during the reduction of graphene oxide, at 17.50 peak also reduce of the portion of the graphene oxide [54]. Thus it was concluded that the reduced graphene oxide was obtained.

TGA curves of raw graphite, GO and rGO are shown in Fig. 1c. TGA curve of raw graphite showed the smallest mass loss in the entire temperature range. The mass loss of GO occurred in different temperature ranges (the first step 0-240 °C and the second 240–450 °C), which was explained by the evaporation of labile oxygen-containing functional groups [55,56]. Thermal stability of red-GO appeared higher than that of pure GO, which indicated the efficient removal of oxygen-containing functional groups by using hydrazine hydrate as the reducing agent. As a result, raw graphite, GO and red-GO showed the respective mass loss as about 4%, 60% and 20% of their own total mass in the entire temperature range.

SEM images of raw graphite, GO and rGO taken in the area of 1 μm are shown in Fig. 2. SEM image of raw graphite showed sharp and regular layers (see Fig. 2a). On the other hand, the SEM image of GO exhibited a disappeared irregular structure (see Fig. 2b). As given in Fig. 2c, nanosheets of red-GO obtained by chemical reduction of the GO showed reoccurrence of distinct layers, which were not as sharp as in the raw graphite.

3.2. Electrochemical properties of the GO/GC and red GO/GC electrodes

Fig. 3a shows that the anodic and cathodic peaks of bare GC, GO/GC and red-GO/GC electrodes were recorded in the presence of 1.0 mM potassium ferricyanide in BR buffer, pH 2.0 solution versus Ag/AgCl/KCl_{sat}. at a scan rate of 100 mV/s using CV. As shown in Fig. 3a couple of well-defined redox peaks were observed for the bare GC electrode (see Fig. 3, red line) because of the reversible redox behavior of the ferricyanide ion. After immobilization of the GO onto the bare GC surface, a largely blocked interfacial charge transfer between the GC surface and ferricyanide ion was observed (see Fig. 3, blue line) due to the GO film acting as a barrier. Compared to the GO and the bare GC surface, CV studies showed that the redox peak current's intensity on the red-GO/GC (see Fig. 3, green line) electrode was higher than those observed for the GO/GC and bare GC surface in cyclic voltammograms. This demonstrated that the reactions of the ferricyanide redox probe were more reversible on the red-GO modified surface than the GO modified surface at the lower pH value (pH 2.0) due to the reduction in the majority-OH groups of the negative charge in the GO structure. Thus the red-GO modified GC electrode showed enhanced peak current and electron transfer rates due to further reduction of GO [57,58]. Then, the charge transport process of bare GC, GO/GC and red-GO/GC surfaces were studied in 100 mM KCl containing 1.0 mM of ferricyanide/ferrocyanide mixture using EIS. Impedance studies showed a decrease in the resistance of the GO/GC surface in Nyquist plots (see Fig. 3b). Because GO enhances the conduction process and thus decreases the resistance for the modified surface. When comparing the red-GO/GC surface with the bare GC surface it was seen that this surface catalyzed the electrons transfer of ferri/ferrocyanide redox couple [58,59]. From CV and EIS studies it is evident that red-GO/GC electrode exhibited a higher conductivity than bare GC and GO/GC electrodes due to the decreased oxygen content of red-GO. CV results were consistent with the EIS results.

3.3. Electrochemical determination of copper ions from different copper salts

The synthesized GO and rGO were used as efficient electrode materials to fabricate a highly sensitive and selective metal sensor for the determination of copper [60]. In order to achieve better sensitivity, DPV was employed as an analytical technique for effective detection of Cu(II) using different copper salt solutions. Fig. 4a–c show DPV responses of bare GC, GO/GC and red-GO/GC surfaces respectively in the presence of 1 mM $CuSO_4{\cdot}5H_2O$, $Cu(NO_3)_2{\cdot}3H_2O$ and $CuCI_2$ salt solutions

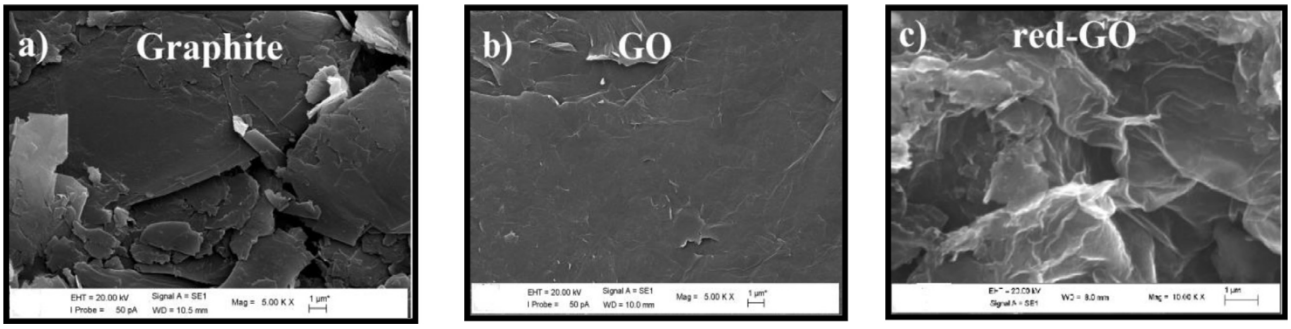

Fig. 2. SEM micrographs of (a) Graphite, (b) GO, (c) red-GO.

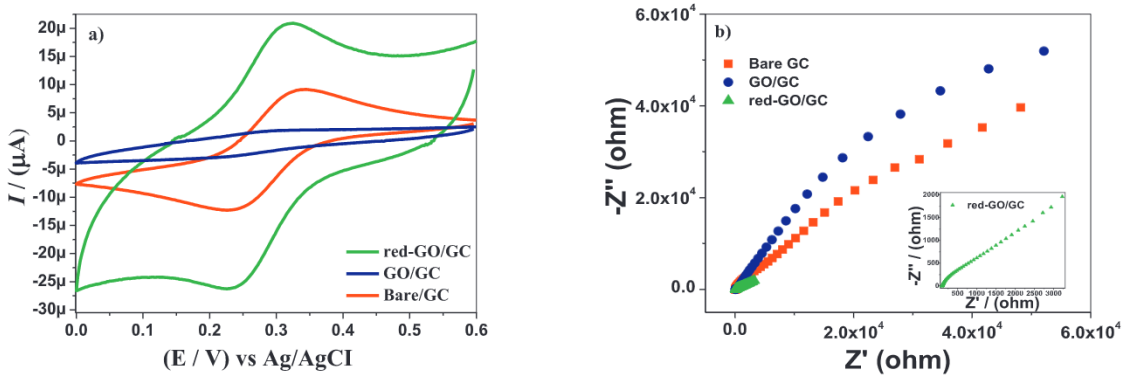

Fig. 3. (a) Cyclic voltammograms of 1.0 mM of ferricyanide in BR buffer, pH 2.0 at Bare GC, GO/GC, red-GO/GC surface. Potential sweep rate was 100 mV/s. (b) Nyquist plots of 1.0 mM of ferri/ferrocyanide mixture solution in 100 mM of KCl Bare GC, GO/GC, red-GO/GC at frequency range from 0.1 Hz to 75 kHz.

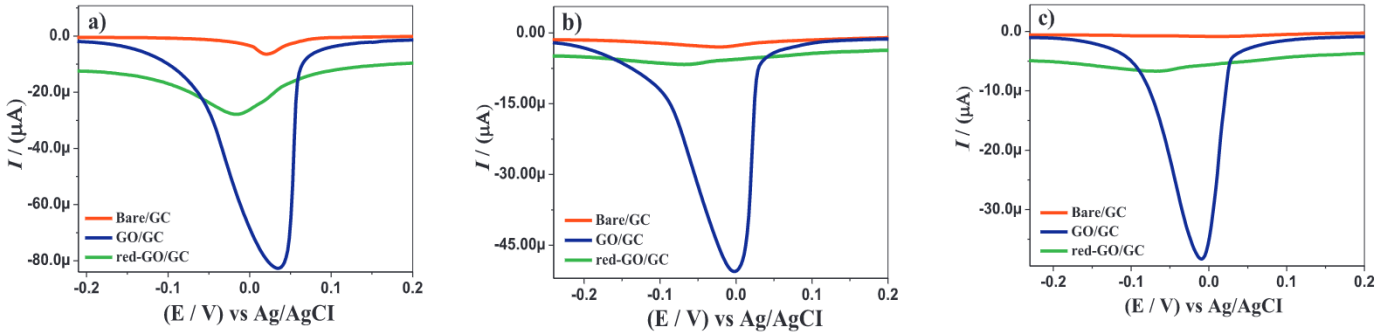

Fig. 4. Differential pulse voltammograms of Cu(II) at Bare GC; GO/GC; red-GO/GC recorded in BR buffer solution, pH 5.0. in the solution prepared with the (a) copper nitrate salt, (b) copper sulfate salt, (c) copper chloride salt.

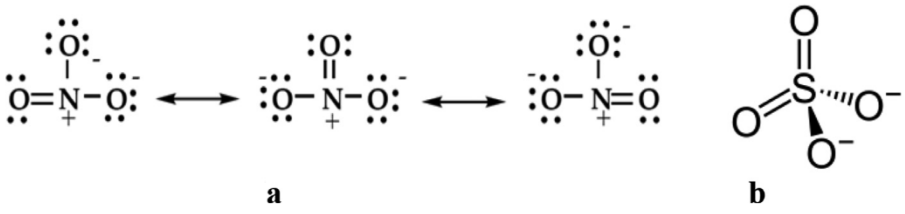

Fig. 5. (a) Resonance structure of nitrate ion, (b) Structure of sulfate ion.

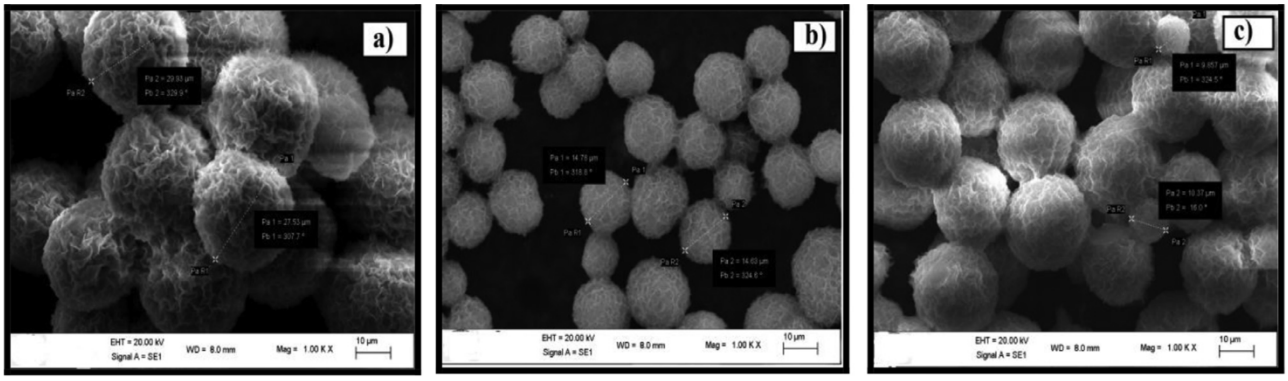

Fig. 6. SEM image of the aggregation formed by Cu (II) ions on GO/GC surface after standing in (a) the copper nitrate, (b) the copper sulfate, (c) the copper chloride solutions prepared in buffer BR at pH 5.0.

prepared in BR buffer, pH 5.0. The peaks with different sensitivity for Cu(II) ions were detected versus $Ag/AgCl/KCl_{sat}$ on these surfaces. DPV voltammograms showed that the highest sensitivity was at the surface of the GO/GC electrode. This is thought to be due to the negatively charged groups in the GO structure. Other researchers also noticed that GO is focused on this effect of negative groups on GO structure in copper ions determination [61,62]. For $CuSO_4{\cdot}5H_2O$, $Cu(NO_3)_2{\cdot}3H_2O$ and $CuCl_2$ salts, the peaks were observed respectively at 0.0012 V, 0.0346 V, and 0.0008 V with the sensitivity of 50.56 μA 82.60 μA, and 38.17 μA at the GO/GC surface.

The effect of anion roots, focusing on the effect of the salt was also investigated. At this point, when the sensitivity of the GO/GC electrode to copper ions was examined, it was determined that the electrochemical responses of salts were $Cu(NO_3)_2 > CuSO_4 > CuCl_2$. Thus it

Table 1
Interference of various metal ions to DPV signal of GO/GC electrode registered in BR buffer, pH 5.0 vs. Ag/AgCl/KClsat.

Ions	Concentration (mM)	DPV peak curent (μA)	Relative difference from 1 mM Cu^{2+}
Cu(II)	1	−82,05	0
All metals	1	−62,98	23,24
Zn	1	52,40	36,48
Pb	1	48,36	41,06
Cd	1	50,17	38,85
Fe	1	36,48	55,53
Mn	1	42,31	48,43

was thought that Pearson's hard acid-base theory can explain the effects of anion/anion groups on determination of Cu(II) ions. According to Pearson, the hard base that is large in ionic potential and the hard acid that is large in ionic potential, and similarly the soft base that is small in ionic potential and the soft acid that is small in ionic potential are thermodynamically more stable [63]. When all these factors are taken into consideration, the hardness status of the structures used in the study according to Pearson is listed below.

Cu^{+2} →medium hard acid SO_4^{-2} →hard base NO_3^- → hard base CI^- →hard base

The Cu^{+2} cation is (medium) hard acid and contains d orbitals. Because of the low shielding effect [S] of d orbitals the effective core charge [Z*] of Cu^{2+} is greater than the apparent force, the radius is small and it has large ionization potential [ϕ]. Chloride (Cl^-), nitrate (NO_3^-) and sulfate (SO_4^{-2}) anion/anion groups are hard bases with high ionic potentials (ϕ). In this case (hard acid-hard base) all of them appear to be thermodynamically stable. The difference between them determines that anion/anion groups are arranged in terms of their susceptibility to the metal ions of the donor atoms [64]. The chloride anion is larger than the ionic potential of nitrate and sulfate anion groups (harder base) attached to O^{-2} and $CuCl_2$ is the most stable structure thermodynamically [50]. For this reason, it can be said that the electrochemical responses of $CuCl_2$ are lower. Also, we can explain nitrate and sulfate hard bases that have lower ionic potentials with their π bonds, which is one of the reasons that affect hardness-softness properties among themselves. According to Lewis's theory, the nitrate anion has three resonance structures so its base is reduced and the ionic potential is lower (see Fig. 5a). The sulfate anion also has a single structure with a higher ionic potential, which is the harder base (see Fig. 5b). Thus A $CuSO_4$ formed by the Cu^{+2} cation that is a strong acid thermodynamically is more stable than Cu $(NO_3)_2$. For this reason, we can say that the electrochemical response of the sulfate salt is lower. Since the thermodynamic stability order is $Cu(NO_3)_2 < CuSO_4 < CuCl_2$, to give the highest electrochemical response of nitrate salt is a condition that is expected.

3.4. Characterization of electrode surfaces in the presence of Cu(II) by SEM

GO/GC surface was kept in $CuSO_4{\cdot}5H_2O$, $Cu(NO_3)_2{\cdot}3H_2O$ and $CuCI_2$ salt solutions under optimum conditions and SEM images of Cu(II) ions were taken in 10 μm area and the diameters of the agglomerations formed by Cu(II) ions were measured. Fig. 6a shows that Cu(II) ions were deposited in the form of a cauliflower on the 10 μm area and had an average size of 28.75 μm on the GO/GC surface that waited in the Cu $(NO_3)_2{\cdot}3H_2O$ solution. Then Fig. 6b shows that Cu(II) ions scattered as cauliflower appearance with sharp lines and an average size of 14.70 μm on the GO/GC surface that waited in the $CuSO_4{\cdot}5H_2O$ solution. Fig. 6c also shows Cu(II) ions in the form of cauliflower appearance, with markedness lines significantly reduced, densely packed and with an average size of 10.11 μm on the GO/GC surface that waited in the $CuCI_2$ solution.

3.5. Interference studies

Considering that different heavy metals may affect the electrochemical determination of the target ion (Cu(II)), selectivity of GO/GC surface for Cu(II) ions were investigated individually as well as simultaneously by the DPV technique in the presence of interfering Zn (II), Pb(II), Cd(II), Fe(III) and Mn(II) heavy metal ions. When other ions were presented at the same concentration as Cu(II) ions, the order of interference effect was determined as Fe(III) > Mn(II) > Pb(II) > Cd (II) > Zn(II). The presented interfering metal ions at 1 mM concentration reduced the current peak from 36.48 to 55.53%. In case all different metal ions were presented in the same concentration in the media, the developed GO/GC sensor was clearly able to determine Cu (II) ions and the current peak of copper(II) ions reduced to 23.24%. Also, no additional peaks were visible in the related potential range, which would clearly indicate the interference effect and no other peaks were observed in the potential range between −0.3 V and +0.3 V. At this point we can say that Cu(II) ions are more rapidly bound to than other metal functional groups containing -OH on the GO/GC surface. The analytical parameters of Cu(II), Zn(II), Pb(II), Cd(II), and Fe(III) metal ions are presented in Table 1.

Further repeatability and reproducibility of the GO nanoparticle modified GC electrode were evaluated by taking three repetitive measurements of DPV in the presence of 0.1 mM Cu(II) ions. For measurements of repeatability of Cu(II) ions on the GO/GC electrode, the relative standard deviation (RSD) was 5.22, 0.58, and 0.62% for $CuSO_4{\cdot}5H_2O$, $Cu(NO_3)_2{\cdot}3H_2O$, and $CuCI_2$ salts, respectively. Reproducibility of the GO/GC electrode was verified with three different electrodes and it showed an RSD of 0.73, 0.71, and 0.98% for $CuSO_4{\cdot}5H_2O$, $Cu(NO_3)_2{\cdot}3H_2O$, and $CuCI_2$ salts, respectively. The stability of the GO/GC electrode was estimated in the presence of 0.1 mM of Cu(II) in $CuSO_4{\cdot}5H_2O$, $Cu(NO_3)_2{\cdot}3H_2O$, and $CuCI_2$ salt solutions and retained sensitivity of 87.2, 80.1, and 86.3%, respectively for a period of 45 days. The results indicate that the proposed sensor was highly accurate. There was good reproducibility as the obtained relative standard deviations (RSDs) are very small in all salts showing good repeatability of the modified electrodes.

4. Conclusions

The GO/GC electrode proposed in this study showed high electrochemical sensitivity towards Cu(II) ions of different copper salts. The effect of anion roots on Cu^{+2} ions was investigated for the first time in this study. It was demonstrated that the electrochemical responses are consistent with the inorganic theory. Thus a sensor design for the electrochemical characterization of Cu(II) ions from heavy metals, which threaten human and environmental health, was developed opening a new avenue for the development of sensing systems suitable for industrial applications.

Acknowledgment

This research was supported by Selcuk University Research Foundation under the project number 13201024. We would like to thank Selcuk University Research Foundation for their financial support.

References

[1] G. Aragay, A. Merkoçi, Nanomaterials application in electrochemical detection of heavy metals, Electrochim. Acta 84 (2012) 49–61.
[2] A. Pal, J. Jayamani, R. Prasad, An urgent need to reassess the safe levels of copper in the drinking water: lessons from studies on healthy animals harboring no genetic deficits, Neurotoxicology 44 (2014) 58–60.
[3] S.-P. Wu, R.-Y. Huang, K.-J. Du, Colorimetric sensing of Cu (II) by 2-methyl-3-[(*pyridin-2-ylmethyl*)-*amino*]-1, 4-naphthoquinone: Cu (II) induced deprotonation of NH responsible for color changes, Dalton Trans. 24 (2009) 4735–4740.

[4] Y.R. Kim, H.J. Kim, J.S. Kim, H. Kim, Rhodamine-based “turn-on” fluorescent chemodosimeter for Cu (II) on ultrathin platinum films as molecular switches, Adv. Mater. 20 (2008) 4428–4432.
[5] C. Zong, K. Ai, G. Zhang, H. Li, L. Lu, Dual-emission fluorescent silica nanoparticle-based probe for ultrasensitive detection of Cu^{2+}, Anal. Chem. 83 (2011) 3126–3132.
[6] Z. Wang, M. Wang, G. Wu, D. Wu, A. Wu, Colorimetric detection of copper and efficient removal of heavy metal ions from water by diamine-functionalized SBA-15, Dalton Trans. 43 (2014) 8461–8468.
[7] L.M. Niu, H.Q. Luo, N.B. Li, L. Song, Electrochemical detection of copper (II) at a gold electrode modified with a self-assembled monolayer of penicillamine, J. Anal. Chem. 62 (2007) 470–474.
[8] F. Yang, D. He, B. Zheng, D. Xiao, L. Wu, Y. Guo, Self-assembled hybrids with xanthate functionalized carbon nanotubes and electro-exfoliating graphene sheets for electrochemical sensing of copper ions, J. Electroanal. Chem. 767 (2016) 100–107.
[9] J. Higdon, An Evidence-Based Approach to Vitamins and Minerals Health Benefits and Intake Recommendations, Thieme Medical Publishers, Inc., 2003.
[10] H. Kozlowski, M. Luczkowski, M. Remelli, D. Valensin, Copper, zinc and iron in neurodegenerative diseases (Alzheimer's, Parkinson's and prion diseases), Coord. Chem. Rev. 256 (2012) 2129–2141.
[11] A.F. Barbosa, V.M. Barbosa, J. Bettini, P.O. Luccas, E.C. Figueiredo, Restricted access carbon nanotubes for direct extraction of cadmium from human serum samples followed by atomic absorption spectrometry analysis, Talanta 131 (2015) 213–220.
[12] B. Hu, C. Huang, X. Li, G. Sheng, H. Li, X. Ren, J. Ma, J. Wang, Y. Huang, Macroscopic and spectroscopic insights into the mutual interaction of graphene oxide, Cu (II), and Mg/Al layered double hydroxides, Chem. Eng. J. (2016) 527–534.
[13] X. Liao, B. Liang, Z. Li, Y. Li, A simple, rapid and sensitive ultraviolet-visible spectrophotometric technique for the determination of ultra-trace copper based on injection-ultrasound-assisted dispersive liquid–liquid microextraction, Analyst 136 (2011) 4580–4586.
[14] P. Borthakur, G. Darabdhara, M.R. Das, R. Boukherroub, S. Szunerits, Solvothermal synthesis of CoS/reduced porous graphene oxide nanocomposite for selective colorimetric detection of Hg (II) ion in aqueous medium, Sens. Actuators B: Chem. (2017).
[15] P. Rameshkumar, N.M. Huang, L.S. Wei, Visual and spectrophotometric determination of mercury (II) using silver nanoparticles modified with graphene oxide, Microchim. Acta 183 (2016) 597–603.
[16] Z. Hu, J. Hu, Y. Cui, G. Wang, X. Zhang, K. Uvdal, H.-W. Gao, A facile “click” reaction to fabricate a FRET-based ratiometric fluorescent Cu 2+ probe, J. Mater. Chem. B 2 (2014) 4467–4472.
[17] Z.S. Qian, X.Y. Shan, L.J. Chai, J.R. Chen, H. Feng, A fluorescent nanosensor based on graphene quantum dots–aptamer probe and graphene oxide platform for detection of lead (II) ion, Biosens. Bioelectron. 68 (2015) 225–231.
[18] S. Lee, J. Oh, D. Kim, Y. Piao, A sensitive electrochemical sensor using an iron oxide/graphene composite for the simultaneous detection of heavy metal ions, Talanta 160 (2016) 528–536.
[19] Y.-F. Sun, L.-J. Zhao, T.-J. Jiang, S.-S. Li, M. Yang, X.-J. Huang, Sensitive and selective electrochemical detection of heavy metal ions using amino-functionalized carbon microspheres, J. Electroanal. Chem. 760 (2016) 143–150.
[20] J. Chang, G. Zhou, E.R. Christensen, R. Heideman, J. Chen, Graphene-based sensors for detection of heavy metals in water: a review, Anal. Bioanal. Chem. 406 (2014) 3957–3975.
[21] F.R. Baptista, S. Belhout, S. Giordani, S. Quinn, Recent developments in carbon nanomaterial sensors, Chem. Soc. Rev. 44 (2015) 4433–4453.
[22] P. Greil, Perspectives of nano-carbon based engineering materials, Adv. Eng. Mater. 17 (2015) 124–137.
[23] B. Zhang, J. Chen, H. Zhu, T. Yang, M. Zou, M. Zhang, M. Du, Facile and green fabrication of size-controlled AuNPs/CNFs hybrids for the highly sensitive simultaneous detection of heavy metal ions, Electrochim. Acta 196 (2016) 422–430.
[24] Y. Lian, M. Yuan, H. Zhao, DNA wrapped metallic single-walled carbon nanotube sensor for Pb (II) detection, Fullerenes, Nanotubes Carbon Nanostruct. 22 (2014) 510–518.
[25] H. Xing, J. Xu, X. Zhu, X. Duan, L. Lu, Y. Zuo, Y. Zhang, W. Wang, A new electrochemical sensor based on carboimidazole grafted reduced graphene oxide for simultaneous detection of Hg^{2+} and Pb^{2+}, J. Electroanal. Chem. 782 (2016) 250–255.
[26] Q. Tu, C. Tian, T. Ma, L. Pang, J. Wang, Click synthesis of quaternized poly (dimethylaminoethyl methacrylate) functionalized graphene oxide with improved antibacterial and antifouling ability, Colloids Surf. B: Biointerfaces 141 (2016) 196–205.
[27] X. Wang, P. Huang, L. Feng, M. He, S. Guo, G. Shen, D. Cui, Green controllable synthesis of silver nanomaterials on graphene oxide sheets via spontaneous reduction, Rsc Adv. 2 (2012) 3816–3822.
[28] B. Peng, M. Locascio, P. Zapol, S. Li, S.L. Mielke, G.C. Schatz, H.D. Espinosa, Measurements of near-ultimate strength for multiwalled carbon nanotubes and irradiation-induced crosslinking improvements, Nat. Nanotechnol. 3 (2008) 626–631.
[29] V. Singh, D. Joung, L. Zhai, S. Das, S.I. Khondaker, S. Seal, Graphene based materials: past, present and future, Prog. Mater. Sci. 56 (2011) 1178–1271.
[30] C.-H. Tsai, W.-C. Huang, W.-S. Wang, C.-J. Shih, W.-F. Chi, Y.-C. Hu, Y.-H. Yu, Reduced graphene oxide/macrocyclic iron complex hybrid materials as counter electrodes for dye-sensitized solar cells, J. Colloid Interface Sci. 495 (2017) 111–121.
[31] D. Majumdar, N. Baugh, S.K. Bhattacharya, Ultrasound assisted formation of reduced graphene oxide-copper (II) oxide nanocomposite for energy storage applications, Colloids Surf. A: Physicochem. Eng. Aspects 512 (2017) 158–170.
[32] H.G. Shiraz, O. Tavakoli, Investigation of graphene-based systems for hydrogen storage, Renewable Sustainable Energy Rev. 74 (2017) 104–109.
[33] X. Du, I. Skachko, A. Barker, E.Y. Andrei, Approaching ballistic transport in suspended graphene, Nat. Nanotechnol. 3 (2008) 491–495.
[34] S.R. Shin, Y.-C. Li, H.L. Jang, P. Khoshakhlagh, M. Akbari, A. Nasajpour, Y.S. Zhang, A. Tamayol, A. Khademhosseini, Graphene-based materials for tissue engineering, Adv. Drug Delivery Rev. 105 (2016) 255–274.
[35] P. Xiao, N. Yi, T. Zhang, Y. Huang, H. Chang, Y. Yang, Y. Zhou, Y. Chen, Construction of a fish-like robot based on high performance graphene/PVDF bimorph actuation materials, Adv. Sci. 3 (2016), http://dx.doi.org/10.1002/advs.201500438 in press.
[36] K.-H. Liao, Y.-S. Lin, C.W. Macosko, C.L. Haynes, Cytotoxicity of graphene oxide and graphene in human erythrocytes and skin fibroblasts, ACS Appl. Mater. Interfaces, 3 (2011) 2607–2615.
[37] O.N. Ruiz, K.S. Fernando, B. Wang, N.A. Brown, P.G. Luo, N.D. McNamara, M. Vangsness, Y.-P. Sun, C.E. Bunker, Graphene oxide: a nonspecific enhancer of cellular growth, ACS Nano 5 (2011) 8100–8107.
[38] P.J. Wessely, U. Schwalke, Insitu CCVD grown bilayer graphene transistors for applications in nanoelectronics, Appl. Surf. Sci. 291 (2014) 83–86.
[39] L. Galves, J. Wofford, G. Soares, U. Jahn, C. Pfüller, H. Riechert, J. Lopes, The effect of the SiC (0001) surface morphology on the growth of epitaxial mono-layer graphene nanoribbons, Carbon (2017) 162–168.
[40] Q. Yang, J. Wang, W. Zhang, F. Liu, X. Yue, Y. Liu, M. Yang, Z. Li, J. Wang, Interface engineering of metal organic framework on graphene oxide with enhanced adsorption capacity for organophosphorus pesticide, Chem. Eng. J. 313 (2017) 19–26.
[41] M. Jamshidi, M. Ghaedi, K. Dashtian, A. Ghaedi, S. Hajati, A. Goudarzi, E. Alipanahpour, Highly efficient simultaneous ultrasonic assisted adsorption of brilliant green and eosin B onto ZnS nanoparticles loaded activated carbon: artificial neural network modeling and central composite design optimization, Spectrochim. Acta Part A: Mol. Biomol. Spectrosc. 153 (2016) 257–267.
[42] Y. Lei, F. Chen, Y. Luo, L. Zhang, Synthesis of three-dimensional graphene oxide foam for the removal of heavy metal ions, Chem. Phys. Lett. 593 (2014) 122–127.
[43] D.C. Marcano, D.V. Kosynkin, J.M. Berlin, A. Sinitskii, Z. Sun, A. Slesarev, L.B. Alemany, W. Lu, J.M. Tour, Improved synthesis of graphene oxide, ACS nano, 4 (2010) 4806–4814.
[44] Y. Oztekin, Z. Yazicigil, A.O. Solak, Z. Ustundag, Z. Kilic, S. Bilge, Surface modification and characterization of phenanthroline nanofilms on carbon substrate, Surf. Interface Anal. 43 (2011) 923–930.
[45] Y. Oztekin, A. Ramanaviciene, Z. Yazicigil, A.O. Solak, A. Ramanavicius, Direct electron transfer from glucose oxidase immobilized on polyphenanthroline-modified glassy carbon electrode, Biosens. Bioelectron. 26 (2011) 2541–2546.
[46] Y. Oztekin, Z. Yazicigil, Preparation and characterization of a 1, 10-phenanthroline-modified glassy carbon electrode, Electrochim. Acta 54 (2009) 7294–7298.
[47] F.-y. Guo, Y.-g. Liu, H. Wang, G.-m. Zeng, X.-j. Hu, B.-h. Zheng, T.-t. Li, X.-f. Tan, S.-f. Wang, M.-m. Zhang, Adsorption behavior of Cr (VI) from aqueous solution onto magnetic graphene oxide functionalized with 1, 2-diaminocyclohexanetetraacetic acid, RSC Adv. 5 (2015) 45384–45392.
[48] H.-L. Guo, X.-F. Wang, Q.-Y. Qian, F.-B. Wang, X.-H. Xia, A green approach to the synthesis of graphene nanosheets, ACS nano 3 (2009) 2653–2659.
[49] H.-K. Jeong, Y.P. Lee, M.H. Jin, E.S. Kim, J.J. Bae, Y.H. Lee, Thermal stability of graphite oxide, Chem. Phys. Lett. 470 (2009) 255–258.
[50] I. Kaminska, M.R. Das, Y. Coffinier, J. Niedziolka-Jonsson, J. Sobczak, P. Woisel, J. Lyskawa, M. Opallo, R. Boukherroub, S. Szunerits, Reduction and functionalization of graphene oxide sheets using biomimetic dopamine derivatives in one step, ACS Appl. Mater. Interfaces 4 (2012) 1016–1020.
[51] Y. Wang, D. Zhang, J. Wu, Electrocatalytic oxidation of kojic acid at a reduced graphene sheet modified glassy carbon electrode, J. Electroanal. Chem. 664 (2012) 111–116.
[52] C. Zhu, S. Guo, Y. Fang, S. Dong, Reducing sugar: new functional molecules for the green synthesis of graphene nanosheets, ACS nano 4 (2010) 2429–2437.
[53] S. Thakur, N. Karak, Green reduction of graphene oxide by aqueous phytoextracts, Carbon 50 (2012) 5331–5339.
[54] X. Zhang, K. Li, H. Li, J. Lu, Q. Fu, Y. Chu, Graphene nanosheets synthesis via chemical reduction of graphene oxide using sodium acetate trihydrate solution, Synth. Met. 193 (2014) 132–138.
[55] S. Stankovich, D.A. Dikin, G.H. Dommett, K.M. Kohlhaas, E.J. Zimney, E.A. Stach, R.D. Piner, S.T. Nguyen, R.S. Ruoff, Graphene-based composite materials, Nature, 442 (2006) 282–286.
[56] P. Khanra, T. Kuila, N.H. Kim, S.H. Bae, D.-s. Yu, J.H. Lee, Simultaneous biofunctionalization and reduction of graphene oxide by baker's yeast, Chem. Eng. J. 183 (2012) 526–533.
[57] S. Yang, Z. Lu, S. Luo, C. Liu, Y. Tang, Direct electrodeposition of a biocomposite consisting of reduced graphene oxide, chitosan and glucose oxidase on a glassy carbon electrode for direct sensing of glucose, Microchim. Acta 180 (2013) 127–135.
[58] M.A. Tabrizi, J.N. Varkani, Green synthesis of reduced graphene oxide decorated with gold nanoparticles and its glucose sensing application, Sens. Actuators B: Chem. 202 (2014) 475–482.
[59] S. Kumar, G. Bhanjana, N. Dilbaghi, R. Kumar, A. Umar, Fabrication and characterization of highly sensitive and selective arsenic sensor based on ultra-thin graphene oxide nanosheets, Sens. Actuators B: Chem. 227 (2016) 29–34.
[60] S. Xiong, S. Ye, X. Hu, F. Xie, Electrochemical detection of ultra-trace Cu (II) and interaction mechanism analysis between amine-groups functionalized $CoFe_2O_4$/reduced graphene oxide composites and metal ion, Electrochim. Acta 217 (2016)

24–33.
[61] L. Dedelaite, S. Kizilkaya, H. Incebay, H. Ciftci, M. Ersoz, Z. Yazicigil, Y. Oztekin, A. Ramanaviciene, A. Ramanavicius, Electrochemical determination of Cu (II) ions using glassy carbon electrode modified by some nanomaterials and 3-nitroaniline, Colloids Surf. A: Physicochem. Eng. Aspects 483 (2015) 279–284.
[62] R. Hu, H. Gou, Z. Mo, X. Wei, Y. Wang, Highly selective detection of trace Cu^{2+} based on polyethyleneimine-reduced graphene oxide nanocomposite modified glassy carbon electrode, Ionics 21 (2015) 3125–3133.
[63] J.-L. Vigneresse, Evaluation of the chemical reactivity of the fluid phase through hard–soft acid–base concepts in magmatic intrusions with applications to ore generation, Chem. Geol. 263 (2009) 69–81.
[64] B.W. Pfennig, Principles of Inorganic Chemistry, John Wiley & Sons, 2015.